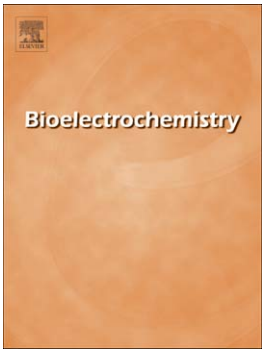

DNA Functionalized Direct Electro-Deposited Gold nanoaggregates for Efficient Detection of Salmonella typhi

Anu Singh, Meenakshi Choudhary, M.P. Singh, H.N. Verma, Surinder P. Singh, Kavita Arora

PII: S1567-5394(15)00029-8
DOI: doi: 10.1016/j.bioelechem.2015.03.005
Reference: BIOJEC 6822

To appear in: *Bioelectrochemistry*

Received date: 27 June 2014
Revised date: 25 March 2015
Accepted date: 26 March 2015

Please cite this article as: Anu Singh, Meenakshi Choudhary, M.P. Singh, H.N. Verma, Surinder P. Singh, Kavita Arora, DNA Functionalized Direct Electro-Deposited Gold nanoaggregates for Efficient Detection of Salmonella typhi, *Bioelectrochemistry* (2015), doi: 10.1016/j.bioelechem.2015.03.005

DNA Functionalized Direct Electro-Deposited Gold nanoaggregates for Efficient Detection of *Salmonella typhi*

Anu Singh[a,b], Meenakshi Choudhary[a], M. P. Singh[a], H. N. Verma[b], Surinder P. Singh[c*], Kavita Arora[a*]
[a] *Advanced Instrumentation Research Facility, Jawaharlal Nehru University, New Delhi-110067*
[b] *School of Life Sciences, Jaipur National University, Jaipur, Rajasthan-302025*
[c] *CSIR-National Physical Laboratory, Dr. K. S. Krishnan Marg, New Delhi –110012*
* *Corresponding authors: kavitaarora@jnu.ac.in, kavitaa@gmail.com, singhsp@mail.nplindia.org*

Abstract

Direct electro-deposition of gold nano-aggregates (GNAs) was carried out to fabricate electrochemical DNA biosensor for the detection of *Salmonella typhi* in urine and blood samples. Size of depositing GNAs was controlled by regulating electro-deposition parameters at physiological pH. This facilitated achieving biocompatible GNAs with desired electrochemical behaviour and enhanced surface area to achieve higher DNA loading. *Salmonella typhi* (*S. typhi*) specific 5'amine modified single stranded DNA (ssDNA, NH_2-(C_6)-5'CGTGCGCGACGCCCGCCGCC3') was covalently immobilized on to GNAs-ITO (indium tin oxide) electrode. Dynamic detection range of 4 aM – 24 fM using methylene blue (MB) redox indicator at 25ºC was achieved using ssDNA-GNAs-ITO bio-electrode to detect the complimentary target sequence (5'GGCGGCGGGCGTCGCGCACG 3') through differential pulse voltammetry (DPV) and electrochemical impedance spectroscopy (EIS). Selectivity of designed electrode was ascertained by the response signal for complementary, non-complementary and 1 base mismatch sequences. Furthermore, clear distinction in complementary and non-complimentary targets was obtained by EIS studies for genomic DNA in culture spiked biological fluids 'CSBF' (blood and urine). This study for detection of *S. typhi* from urine and blood samples using fabricated ssDNA-GNA-ITO bio-electrode showed promising results and have potential to be used as sensors for real patient samples.

Key words: Gold nano-aggregates, DNA biosensor, Electrochemical, Typhoid, Genomic DNA.

1. Introduction

Typhoid fever is a systemic disease caused by Gram-negative pathogen *Salmonella* enteric serovars Typhi (*S. typhi*) [1] which is generally transmitted through ingestion of contaminated food and water [2]. Till date blood culture is the gold standard test for typhoid detection, which is time taking, labour intensive and often exhibit questionable sensitivity in prolonged infection. Available advanced methods like polymerase chain reaction (PCR) and quantitative-PCR [3] are faster but expensive and require skilled manpower. Additionally, the most popular 'Widal Test' identifies the presence of antibodies against *Salmonella* specific O (somatic) and H (flagellar) antigens in the serum that appear only in 2nd week after disease onset [4]. This test is often influenced by other infections like brucellosis, hepatitis and malaria, which mimics the enteric fever and results in false positive [5]. *In spite* of many technological developments, morbidity and mortality rate of typhoid is on rise worldwide.

Development of a rapid and sensitive method/technology for '*on-site*' detection at early stage of disease/ infection is indispensable to combat morbidity and mortality caused by typhoid fever [6]. Biosensors provide promising option for faster and cost-effective analyte detection with desired sensitivity, selectivity that can be implemented for simultaneous monitoring of a wide range of vital pathologic parameters [7]. Various biomolecules such as enzymes, antibodies, nucleic acids and other biological/synthetic/semi-synthetic materials have been widely used to develop biosensors for specific analyte detection [8-9]. Nucleic acid based biosensors are preferred method of choice where immunoglobulin based response cannot be implemented. Especially here, in case of typhoid fever where actual response to the disease can only be traced in its advanced stage i.e. after at least 2 weeks of infection. Keeping favourable electrochemical properties electrochemical transduction is expected to ensure good DNA based sensing research [10]. Various DNA based electrochemical biosensors are summarised in Table 1. Furthermore, performance and capabilities of electrochemical biosensors can be manifold improved by integrating nanotechnology and nanomaterials. Nano based research has already stridden towards improved therapeutics [11] and diagnostics [12] through uniquely designed and engineered nanomaterials. Metal nanoparticles such as gold modified electrodes have been widely investigated and known to enhance the electron transfer between transducer and biomolecule, contributing to improved/ efficient signal transduction and detection signal [13]. Besides this, size/shape of gold nanoparticles critically affects electrochemical behaviour of entire system [14]. Enormous reports have shown potential applications of gold nanostructures for improved electrochemical biosensor. Zhang et. al., 2011 reported electrochemical detection of sequence-specific DNA with amplification of gold nanoparticles having detection limit of 1.7×10^{-13} M using adriamycin as indicator using DPV [15]. Electrically controllable magnetic gold electrode based electrochemical biosensor for single nucleotide polymorphisms (SNPs) from HIV-related salivary DNA has been developed in linear range of 1–100 fM with detection limit of 0.37 fM [16]. Lin et. al., 2011 described electrochemical DNA sensor using assembly of graphene and DNA-conjugated gold nanoparticles through silver enhancement strategy showing detection limit of 72 pM using DPV [17]. Most of these reported strategies are restricted to limited stability, DNA leaching (due to non-covalent interactions/adsorption) stearic hindrances in thiolated DNA probes and limited studies carried out in biological fluids.

In present work, we report fabrication of a simple and stable electrochemical DNA sensor for typhoid detection (Scheme 1) using direct electro-deposited gold nano-aggregates (GNAs) onto ITO substrates. The DNA sensor has been fabricated by covalent immobilization of 5' amine modified ssDNA probe (specific to *S. typhi*) onto self-assembled monolayer (SAM) of 11-mercaptoundecanoic acid (MUA) on GNAs surface. This ssDNA-GNAs-ITO bio-electrode was subsequently exposed to complementary target for hybridization detection studies using DPV in buffer and culture spiked biological fluids (CSBF i.e., blood and urine). GNAs prepared electrochemically at physiological pH (in non toxic solution) enhance the electrochemical behaviour and surface to volume ratio of the electrode providing high loading of ssDNA probe.

2. Experimental

2.1. Consumables and Reagents

Indium tin oxide (ITO) glass plates, chloroauric acid ($HAuCl_4$), phosphate buffer (PB), phosphate buffer saline (PBS), 11-mercaptoundecanoic acid (MUA), 1-(3-dimethylaminopropyl)-3-ethyl-carbodiimide (EDC), N-hydroxysulfosuccinimide (NHS), methylene blue (MB), potassium ferri cyanide [$K_3Fe(CN)_6$)], potassium ferrous cyanide [$K_4Fe(CN)_6.3H_2O$], potassium chloride (KCl), ethanolamine, acetone, trichloroacetic acid (TCA) and DNA sequences were purchased from Sigma-Aldrich. Electrochemical cell consisting homemade Ag/AgCl as reference, Pt wire as counter/auxillary and ITO glass plate as working electrode were also obtained from Sigma Aldrich. Cell cultures (*S. typhi*, *S. paratyphi A, E. coli*) were purchased from MTCC, IMTECH Chandigarh, India and revived in luria broth (LB). Sterile saline water used for all the experiments was from Nirlife healthcare, Nirma Ltd.

The DNA sequences used for electrochemical DNA hybridization detection are as follows:

- ssDNA Probe: NH_2-(C_6)-5'CGTGCGCGACGCCCGCCGCC3' specific to *S. typhi* was selected from conserved Vi capsular antigen gene region of *S. enteric* serovars *typhi* and analyzed through BLAST [http://blast.ncbi.nlm.nih.gov/]. It is worth mentioning that this sequence does not match to any other related species of family Enterobacteriaceae as well as with other micro-organisms.
- Complementary DNA sequence: 5'GGCGGCGGGCGTCGCGCACG 3'
- Non-complementary DNA sequence: 5'GTAACCTGCCTGTAAGACTG 3'
- 1 base mismatch DNA sequence: 5'GGCGCCGGGCGTCGCGCACG3'

2.2. Direct electrochemical deposition of GNAs onto ITO surface

GNAs were directly deposited onto ITO in 0.1 mM $HAuCl_4$ and 0.05 M phosphate buffer solution at pH =7.5 using cyclic voltammetry (AUTOLAB, Ecochemie, The Netherlands) in potential range of -0.2 to -1.3 V with scan rate of 50 mV s^{-1} at 52 ± 2 ºC. ITO glass plates were sequentially pre-cleaned using ultra-sonication in NH_3–H_2O_2 (1:3), ethanol, and water for 15 minutes each.

2.3. Fabrication of ssDNA-GNAs-ITO bio-electrode

GNAs-ITO electrodes were incubated in MUA (5 mM) for 2 h at 25 ºC to functionalize Au surface with –COOH group *via* formation of self-assembled monolayer (SAM). 5'NH_2 modified ssDNA probes were covalently immobilized on MUA functionalized ITO surface using 0.5 M EDC and 0.1 M NHS for providing intermediary ester linkage to facilitate covalent bonding of –NH_2 and –COOH groups. Furthermore, 30 µL of 0.25 nM ssDNA probe was then placed onto the activated MUA-GNAs-ITO for 1 h at 25 ºC. Thereafter, the electrode was washed with water to remove unbound ssDNA probe and the remaining –COOH active sites onto ssDNA-GNAs-ITO surface were blocked by incubating the electrodes in 100 mM ethanolamine for 30 minutes. The bio-electrodes were washed with sterile water to remove excess ethanolamine and thus prepared ssDNA-GNAs-ITO bio-electrodes were stored at 4 ºC under desiccated condition prior to being used.

2.4. DNA Hybridization

ssDNA-GNAs-ITO bio-electrode surface was hand-spotted with desired concentration of sample solution (diluted in water) and kept at 35 ºC for 60 s. The bio-electrode was analysed for DNA hybridization detection through DPV using methylene blue (MB) as redox indicator. ds/ssDNA-GNAs-ITO bio-electrode was pre-treated with 0.1 mM MB for 1 min to identify hybridization event.

Genomic DNA hybridization detection was analysed using EIS measurements in zobell's solution [5 mM $K_3Fe(CN)_6$ in 0.1M KCl] at 10 kHz - 100 mHz and alternate voltage of 5 mV. 5 mL

volume of both urine and blood samples from a healthy individual was spiked with 100 µL of bacterial culture (*S. typhi*) [6.2×10^9 CFU mL^{-1} at 1/10 OD of 0.8, calculated using serial dilution method]. The culture spiked biological fluids (CSBF) samples were centrifuged at 2000 rpm for 20 min and re-suspended in 200 µL of TE buffer (50 mM Tris and 10 mM EDTA, pH =7.5). These samples were sonicated for 3 min to obtain fragmented DNA strands. Further, 10 % TCA in acetone (chilled) was added to it and mixture was. This was followed by incubation at -20 °C for 3 h to remove proteinaceous contamination. The solution was later on centrifuged at 15000 rpm for 30 min and supernatant was collected for further DNA hybridization detection. Hereafter, total DNA extracted is denoted as N.

3. Results and Discussions

3.1. Electrochemical and structural characterization of GNAs-ITO electrode

GNAs have been successfully deposited onto ITO at physiological pH (50 mM phosphate buffer, pH =7.4) using cyclic voltammetry avoiding use of toxic ions such as cyanide [18] (Fig. 1a). It can be seen that during first deposition cycle, forward scan is crossed by reverse scan which is in agreement with the typical metallic deposition process prior to nucleation [19]. Thereafter, peak shift in subsequent cycles towards lower potential (-0.8 V to -0.95 V) depicting nucleation process of GNAs onto ITO surface. Fig. 1b, shows CV studies of fabricated GNAs-ITO electrode in PBS revealing a characteristic pair of oxidation (~0.70 V) and reduction (~0.127 V) peaks due to the formation of soluble Au (III) chloride complexes indicating successful deposition of nano-structured gold aggregates onto ITO surface [20]. Fig. 1c reveals electrochemical characterization of bare ITO and GNAs-ITO prepared through 30 deposition cycles using CV in Zobell's solution. It can be seen that peak separation potential (ΔE_p) of GNAs-ITO decreases to 0.191 V compared to 0.225 V of bare ITO due to the formation of GNAs on ITO surface and increase in peak current is ascribed to improved electron transfer rate through the surface.

This GNAs-ITO electrode further subjected to electrochemical characterization using CV at various scan rates (0.02 - 0.16 Vs^{-1}) in Zobell's solution (Fig.1d). It has been observed that redox peaks are roughly symmetric at low scan rates and peak separation potential (ΔE_p) increases with the scan rate (v). At the same time, redox peak current increases linearly with square root of scan rate having regression coefficient (R^2) 0.997 and 0.990 for I_{pa} and I_{pc}, respectively (Fig 1d: inset). Moreover, at low scan rate the ratio of peak currents (I_{pa}/I_{pc}) is 1.07, (which is close to 1), suggests GNAs-ITO electrode exhibit reversible electron transfer behaviour [18]. The electroactive areas of both bare ITO and GNAs-ITO electrodes have been calculated using Randal-Sevcik equation (1) for planar electrodes [19]:

$$I_p = (2.69 \times 10^5)\, n^{3/2} A D^{1/2} C v^{1/2} \qquad \ldots (1)$$

Where I_p refers to the anodic peak current, A is the surface area of the electrode, D is diffusion coefficient, c is concentration of $K_3Fe(CN)_6$ in mM, v is scan rate in $Vs^{-1}$and here n is 1 electron. Among these parameters, D value of 0.65×10^{-5} cm^2 s^{-1} at 25 °C [20] has been used for the system containing 5 mM $K_3Fe(CN)_6$ in 0.1M KCl as supporting electrolyte. The electroactive area for GNAs-ITO has been found to be 0.11578 cm^2 as compared to 0.102869 cm^2 of bare ITO indicating 12.62 % increase due to GNAs deposition.

Surface coverage was determined using the expression $Q = nFA\tau$, where Q is the amount of charge (C), τ the surface coverage (mol cm^{-2}), n the number of electrons involved in the electron-transfer process, A is the electroactive surface area (cm^2), and F is the Faraday constant [21]. Calculated τ value of 4.05×10^{-7} mol cm^{-2} for GNAs-ITO is 100 times greater than that of 4.41×10^{-9} mol cm^{-2} for bare ITO.

Here Fig. 1

GNAs-ITO electrodes deposited with 20, 30 and 40 CV deposition cycles were characterized using CV, X-ray diffraction (XRD) and DPV studies. CV studies (Fig. S1) of GNAs-ITO shows increase in peak current with increasing number of deposition cycles that can be ascribed to improved electron transfer through surface during progressive gold deposition. XRD pattern of bare ITO and GNAs-ITO deposited for 20, 30 and 40 cycles is shown in Fig. S2. The characteristic diffraction peaks of Au at 38.172º & 44.257º Bragg's angle (2θ) were not observed for bare ITO and for 20 cycles of GNAs deposition. However, the diffraction peak at 38.172º started appearing for GNAs-ITO deposited for 30 cycles. The distinct diffraction peaks at 38.172º & 44.257º corresponding to (111) and (002) planes of face centered cubic (fcc) polycrystalline gold with lattice constant 4.084 Å (ICSD: - 98-006-1206) were obtained for 40 cycle deposition. Crystallite size of GNAs for (111) peaks were calculated to be 7.9 nm and 13.5 nm for 30 and 40 deposition cycles respectively, using Scherer's formula. This suggests that GNAs deposited for 30 cycles possess higher surface area compared to 40 cycle deposition. The increasing oxidation current for gold nano-aggregates deposited onto ITO surface (Fig. S1) could be attributed to proper phase formation of GNAs with increase in the number of deposition cycle [22]. It has been further established that ssDNA is successfully immobilized onto GNAs-ITO electrode deposited for 20, 30, 40 CV cycles (Fig. S3), as characteristic peak for MB has been obtained at -0.35 V in DPV studies [23] which is absent for GNAs-ITO electrode. Additionally, highest peak current (I_p) has been obtained for ssDNA-GNAs-ITO bio-electrode fabricated by 30 deposition cycles of GNAs compared to 20 & 40 deposition cycles (Fig. S3). It may be noted that GNAs-ITO electrode with 30 deposition cycles provides higher surface area compared to 40 deposition cycles resulting in higher loading of biomolecule of choice. Therefore, GNAs-ITO electrode deposited for 30 deposition cycles has been selected for further experimental investigations.

3.2. Morphological characterization of GNAs-ITO electrode deposited for 30 CV cycles

Morphological characterization of bare ITO and GNAs-ITO electrode using scanning electron microscopy (SEM) and atomic force microscopy (AFM) are shown in Fig. 2 a&b, respectively. It can be seen in both pictures that gold aggregates are uniformly distributed throughout the electrode. SEM pictures reveal that the aggregates are spherical in shape. Supportive EDX results for SEM studies have been additionally shown in Fig. S4. Furthermore, AFM pictures reveal that the roughness of the surface increased from 0.081 to 1.589 nm due to deposition of GNAs and these observed humps like spherical structures are in agreement to SEM studies.

Here Fig. 2

3.3. Electrochemical Characterization of ssDNA-GNAs-ITO bio-electrode

Fig. 3a illustrate DPV studies of bare ITO, GNAs-ITO, MUA functionalized GNAs-ITO and ssDNA-GNAs-ITO bio-electrode. It has been observed that bare ITO does not show oxidation peak whereas distinct oxidation peaks were obtained at 0.701 V, 0.927 V and 1.002 V for GNAs-ITO, MUA functionalized GNAs-ITO and ssDNA-GNAs-ITO bio-electrode, respectively. It may be illustrated here that peak at 0.701 V for GNAs-ITO is due to oxidation of gold; peak at 0.927 V is due to oxidation of MUA functional groups present in MUA-GNAs-ITO electrode. The peak at 1.002 V is due to oxidation of guanine bases present in DNA of ssDNA-GNAs-ITO bio-electrode [24]. Immobilization of ssDNA onto GNAs-ITO electrode has been further attested using electro-active indicator MB, which is known to bind single stranded DNA [23]. GNAs-ITO and MUA-GNAs-ITO does not show any peak for MB oxidation whereas the presence of characteristic peak of MB obtained at -0.35 V in DPV studies for ssDNA-GNAs-ITO electrode confirms the binding of ssDNA onto GNAs-ITO (Fig. 3b).

Here Fig. 3

3.4. Response studies of ssDNA-GNAs-ITO bio-electrode

Fig. 4a&b describes the DPV response studies of ssDNA-GNAs-ITO bio-electrode by using MB as hybridization indicator. Fig. 4a, depicts DPV response curves of ssDNA-GNAs-ITO bio-electrode for DNA hybridization with complementary, non-complementary and one base mismatch sequence (50 fM each) by using MB as redox indicator. MB is generally used as an electrochemical indicator to study the DNA hybridization since ssDNA and dsDNA have different affinities. MB had a higher affinity for ssDNA compared to that for dsDNA because it has a strong affinity for free guanine bases [25] leading to decrease in peak current for dsDNA in comparison to ssDNA. It is evident from the response curves that peak current decreases from 82 µA to 27.3 µA when ssDNA-GNAs-ITO bio-electrode hybridizes with complementary sequence. This decrease in peak current may be attributed to the fact that in dsDNA free electron hopping is not readily available [24] as compared to ssDNA. While after hybridization with non complementary sequence no significant change in current has been observed. Furthermore, there is a nominal decrease in peak current after hybridization with 1 base mismatch sequence which can be accredited to mismatch formed at the proximal end, i.e. closer to the GNAs-ITO surface and away from the oligonucleotide monolayer/solution interface. As mismatch cause the unpaired ends of the target strands to occupy more space than if it was hybridized, the proximal mismatch is restrained and feels stronger repulsions from neighbouring probe strands, thus decreasing the rate of formation of the duplex and its stability [26]. The results clearly indicate that ssDNA-GNAs-ITO bio-electrode exhibits good selectivity towards target and non-target sequences. Fig. 4b shows response curves of ssDNA-GNAs-ITO bio-electrode for various concentrations of complementary sequence in the dynamic range 4 aM- 24 fM and follows linear equation (Fig. 4c) I (µA) = 9.132 – 1.479 log c, with a correlation coefficient of 0.9857.

Here Fig. 4

A comparison of performance characteristics of recently reported electrochemical DNA biosensors is shown in Table 1. Detection of low concentration of complementary sequence is attributed to higher surface area provided by uniformly distributed spherical nano-aggregates and longer linker threads, facilitating free movement/interaction of ssDNA probe (as shown in Scheme 1) with complementary target.

Here Table 1

3.5. Stability, reproducibility and regeneration studies of ssDNA-GNAs-ITO bio-electrode

ssDNA-GNAs-ITO bio-electrodes have been subject to stability studies for 60 days while storing at 4 ºC under desiccated condition. DPV response curves of ssDNA-GNA-ITO bio-electrodes were recorded in triplicate, monitoring MB oxidation in PBS for detection of complementary (1 nM) and non-complementary (1 nM) sequence after every 15 days. It is observed that DPV signal recorded at an interval of 0-15 days did not show any change in detection signal and thereafter showed 3 % and 8 % loss after 30 and 60 days, respectively (Fig. S5), indicating the possibility of designing a stable bio-electrode.

Reproducibility of the ssDNA-GNAs-ITO bio-electrode has been estimated with two sets of five ssDNA-GNA-ITO bio-electrodes for 50 nM and 50 pM of complementary sequences. Peak current for ssDNA probe and after hybridization with complementary sequence (50 nM and 50 pM) was analyzed and compared for each set of five electrodes, respectively. Interestingly, the observed peak current was found to vary within 5 % range describing consistency in the response signal (results not shown).

The fabricated dsDNA-GNAs-ITO bio-electrode were regenerated by incubating hybridized electrode in hot water (90 °C) for 60 s, i.e., thermal denaturation of DNA to remove bound complementary sequence. This regenerated bio-electrode was further subject to hybridization detection of 1 nM complementary sequence using DPV response analysis. It has been found that

regenerated ssDNA-GNAs-ITO bio-electrode restores ~92 % signal efficiency up to 3rd regeneration and ~78 % up to 6th regeneration compared to first use of ssDNA-GNA-ITO electrode (Fig. S6).

3.6. Response studies of ssDNA-GNAs-ITO bio-electrode in CSBF samples

The performance of ssDNA-GNAs-ITO bio-electrode has been investigated for its application to real sample by spiking bacterial culture (*S. typhi*) in biological fluids (urine and blood) of a normal person. DPV studies of ssDNA-GNA-ITO bio-electrode were carried out after hybridization with fragmented genomic DNA extracted from urine sample in dilution N, N/2, N/4, N/8 (Fig. S7). The MB oxidation peak current was found to be higher for extracted fragmented genomic DNA sample in contrast to observation made for small target sequences as shown in Fig. 4b. The observed change can be assigned to binding of MB molecules to free single-strands of long DNA fragments that is hybridized onto bio-electrode surface (Fig. S8). On the other hand the peak current increased with decrease in concentration of fragmented genomic DNA sample (higher to lower dilution i.e. N to N/8). This observation may be assigned to the fact that low concentration of fragmented genomic DNA increases the chances of target hybridization compared to high concentration in which target accessibility is low. Whereas, slight decrease in peak current after exposure to non-complementary fragmented genomic DNA (*S. paratyphi A*) suggests nominal non-specific hybridization of some very small fragments.

Additionally, electrochemical impedance spectroscopy (EIS) has been performed for response studies of ssDNA-GNAs-ITO bio-electrodes to confirm hybridization of various concentrations (dilutions N, N/2, N/4, N/8) of fragmented genomic DNA extracted from CSBF samples as shown in Fig. 5a&b. EIS studies contains Nyquist plot of *Z'* versus *-Z"* where the diameter of obtained semicircle reflects charge transfer resistance (R_{CT}) of redox conversion of electro-active species $[Fe(CN)_6]^{3-/4-}$ at bio-electrode surface. Fig 5a shows that R_{CT} value of ssDNA-GNAs-ITO electrode is 327 kΩ and after hybridization with N dilution of fragmented genomic DNA isolated from urine, R_{CT} value increased to 1419 kΩ. The R_{CT} value further increased (2551 to 4067 to 7477 kΩ) after hybridization with lowering concentration (i.e. N/2, N/4, N/8, respectively) of fragmented target genomic DNA in agreement with the DPV results as mentioned above (Fig. S7). This observation also correlates to the fact that low concentration of fragmented genomic DNA increases the chances of target hybridization compared to high concentration in which target accessibility is low due to dense clustering of DNA fragments. This observed rise in R_{CT} could also be attributed to increase in negatively charged sugar-phosphate backbone of hybridized DNA onto electrode surface that is repelling the negatively charged $[Fe(CN)_6]^{3-/4-}$ to access reactive centres.

.

Fig. 5b demonstrate EIS studies of ssDNA-GNAs-ITO electrode that R_{CT} value of bio-electrode (342 kΩ) increased to 1474 kΩ after hybridization with N dilution of fragmented target genomic DNA isolated from blood. It is again noticeable here that R_{CT} in Nyquist plots increases (1554 to 2094 to 4326 kΩ) after hybridization with lowering concentration (i.e. N/2, N/4, N/8, respectively) of fragmented genomic DNA. It may be noted that, the results of response curves obtained from blood samples compared to urine samples show asymmetric rise in R_{CT} value which may be accredited to more protein/other molecules contamination. Fig. 5c shows selectivity response of ssDNA-GNAs-ITO bio-electrode when exposed with fragmented genomic DNA isolated from *S. typhi*, *S. paratyphi A* and *E. coli*. It is worth mentioning that ssDNA-GNAs-ITO bio-electrode shows negligible increase in R_{CT} with non-complementary fragmented genomic DNA compared to significant change in R_{CT} value obtained for complementary fragmented target genomic DNA asserting that the designed electrode exhibit high selectivity.

Here Fig. 5

4. Conclusions

A novel DNA bio-electrode based on direct electro-deposited GNAs has been fabricated and demonstrated for electrochemical detection of *S. typhi* in CSBF. GNAs platform fabricated at physiological pH has improvised the DNA based detection system by providing biocompatible environment, high surface area and minimum stearic hindrance leading to effective selectivity and dynamic detection range of 4 aM – 24 fM using MB as redox indicator. Interestingly, this bio-electrode was able to detect *S. typhi* genomic DNA extracted from culture spiked urine and blood samples (CSBFs) using DPV and EIS studies that warrants its scaling up for real patient sample. Besides this, ssDNA-GNAs-ITO bio-electrode also successfully distinguished between genomic DNA of *S. typhi*, *S. paratyphi*, and *E. coli* revealing high specificity. This biosensor could potentially be applied to the detection of other pathogens like *M. tuberculosis, Campylobacter, H. pylori, E. coli* etc. that can serve as technical platform for fabrication of point-of-care diagnostics. However, the integrated use of innovative materials such as peptide nucleic acid (PNA), tailor-made electroactive matrices, microfluidics, MEMS etc. could help to reach new horizons.

5. Acknowledgements

We are thankful to Prof. S. Ghosh, JNU for allowing us to use AFM facility and his student Pawan for helping in the experiments. Surinder P. Singh thanks the support from CSIR network project NanoSHE (BSC0112). DST-PURSE, UPE-1 JNU Capacity Buildup fund, UPE-2 JNU, DBT sponsored projects IYBA-2008 (BT/B1/12/045/2008) and RGYI-2009 (BT/PR13127/GBD/27/195/2009) are duly acknowledged.

6. References

1. C. Kidgell, U. Reichard, J. Wain, B. Linz, M. Torpdahl, G. Dougan, M. Achtman, *Salmonella* typhi, the causative agent of typhoid fever, is approximately 50,000 years old, Infection, Genetics and Evo. 2 (2002) 39 - 45.
2. S. P. Luby, M. K. Faizan, S. P. Fisher-Hoch, A. Syed, E. D. Mintz, Z. A. Bhutta, Risk factors for typhoid fever in an endemic setting, Karachi, Pakistan, Epidemiol. & Inf. 120 (1998) 129 - 38.
3. A. G. Nagarajan, G. Karnam, A. Lahiri, U. S. Allam, D. Chakravortty, Reliable Means of Diagnosis and Serovar Determination of Blood-Borne *Salmonella* Strains: Quick PCR Amplification of Unique Genomic Loci by Novel Primer Sets, J. Clin. Microbiol. 47 (2009) 2435 - 2441.
4. T. E. Tupasi, R. L. Aquino, M. T. Mendoza, C. U. Tuazon, S. Lolekha, Clinical Application of the Widal Test, Phil J Microbiol Infect Dis. 20 (1991) 23 - 26.
5. M. E. Ohanu, A. U. Mbah, P.O. Okonkwo, F.S. Nwagbo, Interference by malaria in the diagnosis of typhoid using Widal test alone. W. Afr. J. Med. 22 (2003) 250 - 252.
6. A. K. Bhunia, United States of America: Springer Science + Business Media, 2008. LLC.
7. A. Cavalcanti, B. Shirinzadeh, M. Zhang, L. C. Kretly, Nanorobot Hardware Architecture for Medical Defense, Sensors 8 (2008) 2932 – 2958.
8. K. Arora, S. Chand, B. D. Malhotra, Recent developments in bio-molecular electronics techniques for food pathogens, Anal. Chim. Acta 568 (2006) 259 – 274.
9. S. K. Arya, S. Saha, J. E. Ramirez-Vick, V. Gupta, S. Bhansali, S. P. Singh, Recent advances in ZnO nanostructures and thin films for biosensor applications: review, Anal. Chim. Acta 737 (2012) 1 – 21.
10. S. Cagnin, M. Caraballo, C. Guiducci, P. Martini, M. Ross, M. S. Ana, D. Danley, T. West, G. Lanfranchi, Overview of Electrochemical DNA Biosensors: New Approaches to Detect the Expression of Life, Sensors 9 (2009) 3122 - 3148.
11. J. L. West, N. J. Halas, Applications of nanotechnology to biotechnology commentary, Curr. Op. in Biotech. 11 (2000) 215 - 217.
12. C. Zandonella, Cell nanotechnology: The tiny toolkit, Nature 423 (2003) 10 - 12.
13. M. Vidotti, R. F. Carvalhal, R. K. Mendes, D. C. M. Ferreira, L. T. Kubota, Biosensors based on gold nanostructures, J. Braz. Chem. Soc. 22 (2011) 3 - 20.
14. A. Bonanni, M. Pumera, Y. Miyahara, Influence of Gold Nanoparticle Size (2-50 nm) upon its Electrochemical Behavior: An Electrochemical Impedance Spectroscopic and Voltammetric Study, Phys. Chem. Chem. Phys. 13 (2011) 4980 - 4986.

15. Y. Zhang, Z. Wang, Y. Wang, L. Huang, W. Jiang, M. Wang, Electrochemical Detection of Sequence-Specific DNA with the Amplification of Gold Nanoparticles, Int. J. Electrochem. 2011.

16. J. Zhang, X. Y. Wu, W. Yang, J. H. Chen, F. F. Fu, Ultra-sensitive electrochemical detection of single nucleotide polymorphisms based on an electrically controllable magnetic gold electrode. Chem. Commun. 49 (2013) 996 – 998.

17. L. Lin, Y. Liu, L. Tang, J. Li, Electrochemical DNA sensor by the assembly of graphene and DNA-conjugated gold nanoparticles with silver enhancement strategy, Analyst 136 (2011) 4732 - 4737.

18. J. Wang, 2006. Analytical Electrochemistry 3rd Edition. WILEY-VCH, New York.

19. J. E. B. Randles, A cathode ray polarograph, Trans. Faraday Soc. 44 (1948) 322 – 327.

20. C. H. Hamann, A. Hamnett, W. Vielstich, Electrochemistry, Wiley/VCH, Weinheim, Germany, 1998.

21. R.S. Nicholson. Theory and application of cyclic voltammetry for measurements of electrode reaction kinetics. Anal. Chem. 37 (1965) 1351-1355.

22. X. Yu, L. Wang, J. Di, Electrochemical deposition of high density gold nanoparticles on indium/tin oxide electrode for fabrication of biosensors, J. Nanosci. Nanotechnol. 11 (2011) 11084-11088.

23. N. Prabhakar, K. Arora, H. Singh, B. D. Malhotra, Polyaniline based nucleic acid sensor, J. Phys. Chem. B 112 (2008) 4808 - 4816.

24. G. Chiti, G. Marrazza, M. Mascini, Electrochemical DNA biosensor for environmental monitoring, Anal. Chim. Acta 427 (2001) 155 - 164.

25. A. Sassolas, B. D. L. Bouvier, L. J. Blum, DNA Biosensors and Microarrays, Chem. Rev. 108 (2008) 109 − 139.

26. E. Milkani, A. M. Khaing, S. Morais, C. R. Lambert, W. G. M. Gimpsey, SPR based single nucleotide mismatch biosensor, Anal. Methods 3 (2011) 122 – 132.

27. W. Sun, P. Qin, H. Gao, G. Li, K. Jiao, Electrochemical DNA biosensor based on chitosan/nano-V_2O_5/MWCNTs composite film modified carbon ionic liquid electrode and its application to the LAMP product of Yersinia enterocolitica gene sequence, Biosens. Bioelectron. 25 (2010) 1264-1270.

28. E. Spain, R. Kojima, R. B. Kaner, G. G. Wallace, J. O. Grady, K. Lacey, T. Barry, T. E. Keyes, R. J. Forster, High sensitivity DNA detection using gold nanoparticle functionalised polyaniline nanofibres, Biosens. Bioelectron. 26 (2011) 2613 - 2618.

29. Y. Bo, H. Yang, Y. Hu, T. Yao, S. Huang, A novel electrochemical DNA biosensor based on graphene and polyaniline nanowires, Electrochim. Acta 56 (2011) 2676–2681.

30. S. Siddiquee, N. A. Yusof, A. B. Salleh, S. G. Tan, F. A. Bakar, Development of electrochemical DNA biosensor for Trichoderma harzianum based on ionic liquid/ZnO nanoparticles/chitosan/gold electrode, J. Solid State Electrochem. (2012) 1 - 10.

31. A. Ulianas, L. Y. Heng, S. A. Hanifah, T. L. Ling, An Electrochemical DNA Microbiosensor Based on Succinimide-Modified Acrylic Microspheres, Sensors 12 (2012) 5445-5460.

32. A. Singh, G. Sinsinbar, M. Choudhary, V. Kumar, R. Pasricha, H.N. Verma, S. P. Singh, K. Arora, Graphene oxide-chitosan nanocomposite based electrochemical DNA biosensor for detection of typhoid, Sens. Actuators B 185 (2013) 675–684.

33. H. Jin, M. Wei, J. Wang, Electrochemical DNA biosensor based on the BDD nanograss array electrode, Chem. Cent. J. 7 (2013) 65.

34. S. W. Dutse, N. A. Yusof, H. Ahmad, M. Z. Hussein, Z. Zainal, R. Hushiarian, DNA-based Biosensor for Detection of Ganoderma boninense, an B Oil Palm Pathogen Utilizing Newly Synthesized Ruthenium Complex [Ru(phen)2(qtpy)]2+ Based on a PEDOT-PSS/Ag Nanoparticles Modified Electrode, Int. J. Electrochem. Sci., 8 (2013) 11048 – 11057.

35. X. Han, X. Fang, A. Shi, J. Wang, Y. Zhang, An electrochemical DNA biosensor based on gold nanorods decorated graphene oxide sheets for sensing platform, Anal. Biochem. 443:2 (2013) 117-123.

36. C. Liu, D. Jiang, G. Xiang, L. Liu, F. Liu, X. Pu, An electrochemical DNA biosensor for the detection of Mycobacterium tuberculosis, based on signal amplification of graphene and a gold nanoparticle–polyaniline nanocomposite, Analyst 139:21 (2014) 5460-5465.

37. N. A. Mansor, Z. M. Zain, H. H. Hamzah, M. S. A. Noorden, S. S. Jaapar, V. Beni, Z. H. Ibupoto, Detection of Breast Cancer 1 (BRCA1) Gene Using an Electrochemical DNA Biosensor Based on Immobilized ZnO Nanowires, Open J. Appl. Biosens. 3 (2014) 9-17.

38. X. Cao, Ultra-sensitive electrochemical DNA biosensor based on signal amplification using gold nanoparticles modified with molybdenum disulfide, graphene and horseradish peroxidise, Microchim. Acta 181 (2014) 1133–1141.

List of Figures

Scheme1. Methodology for electrochemical DNA biosensor fabrication: (a) Gold nano-aggregates were directly electrodeposited onto ITO (section 2.2); (b) surface functionalization of GNAs using 11-mercaptoundecanoic acid to provide carboxyl functional groups for DNA immobilization (section 2.3); (c) Covalent immobilization of 5'amine modified ssDNA probe onto SAM using EDC-NHS (section 2.3), (d) DNA hybridization with complementary target (section 2.4) and (e) Electrochemical response measurements using DPV for DNA hybridization detection using MB as redox indicator where magnitude of peak current corresponds to the oxidation of MB (section 2.4).

Fig.1. CV curves showing: (a) direct electrochemical deposition of GNAs onto ITO (0.8 × 0.6 cm) in 0.1 M $HAuCl_4$ dissolved in 0.05 M phosphate buffer (pH =7.4) for 1^{st}, 2^{nd}, 10^{th} and 30^{th} cycle (curve 1, 2, 3, 4, respectively) at 52 ± 2 ^{o}C, (b) bare ITO (curve 1) and GNAs-ITO (curve 2) electrode in 0.05 M PBS (pH =7.4) at 50 mV s^{-1}, (c) bare ITO (curve 1) and GNAs-ITO (curve 2, 30 cycle deposition) in zobell's solution at 20 mV s^{-1} and (d) GNAs-ITO electrode at 0.02-0.16 V s^{-1} in zobell's solution, Inset: Plot of anodic peak current I_p versus $v^{½}$ with R^2 0.997 and 0.990 for I_{pa} and I_{pc}, respectively.

Fig.2 (a) SEM and (b) AFM images of bare ITO and GNAs-ITO electrode along with AFM parameters.

Fig.3. DPV studies of (a)bare ITO (curve 1), GNAs-ITO (curve 2), MUA functionalized GNAs-ITO (curve 3) and ssDNA-GNAs-ITO bio-electrodes (curve 4) in 0.05 M PBS (pH =7.4) and (b) GNAs-ITO (curve 1), MUA functionalized GNAs-ITO (curve 2) and ssDNA-GNAs-ITO bio-electrodes (curve 3) in 0.05 M PBS (pH =7.4) using 0.1 mM MB pre-treatment (1 min) at 50 mV pulse height and 70 ms pulse width.

Fig.4. DPV response curves of ssDNA-GNAs-ITO bio-electrode in PBS (0.05 M, pH =7.4) using MB redox indicator at pulse height 50 mV and pulse width 70 ms: (a) ssDNA-GNAs-ITO bio-electrode (curve 1) after hybridization with non complementary, complementary and one base mismatch targets, 50 fM each (Curve 2, 3, 4, respectively); (b) ssDNA-GNAs-ITO bio-electrode (curve 1) after hybridization with 24 fM, 4 fM, 2 fM, 500 aM, 250 aM, 125 aM, 62 aM, 32 aM, 16 aM, 8 aM, 4 aM (curve 2, 3, 4, 5, 6, 7, 8, 9, 10, 11 & 12, respectively) of complementary target and (c) plot of peak current v/s logarithm of the target DNA concentration.

Fig.5. Nyquist plots of ssDNA-GNAs-ITO bio-electrode (curve 1) after hybridization with dilutions N (curve 2), N/2 (curve 3), N/4 (curve 4), N/8 (curve 5) of *S. typhi* genomic DNA obtained from (a) urine samples, (b) blood samples in Zobell's solution in frequency range 10 kHz to 100 m Hz & alternate voltage of 5 mV and (c) Plot of R_{CT} values of ssDNA-GNAs-ITO (Control) and ssDNA-GNA-ITO bio-electrode hybridized with genomic DNA of *S. typhi*, *E. coli* and *S. paratyphi A*. Error bars represent the standard deviation of three replicates.

Graphical abstract

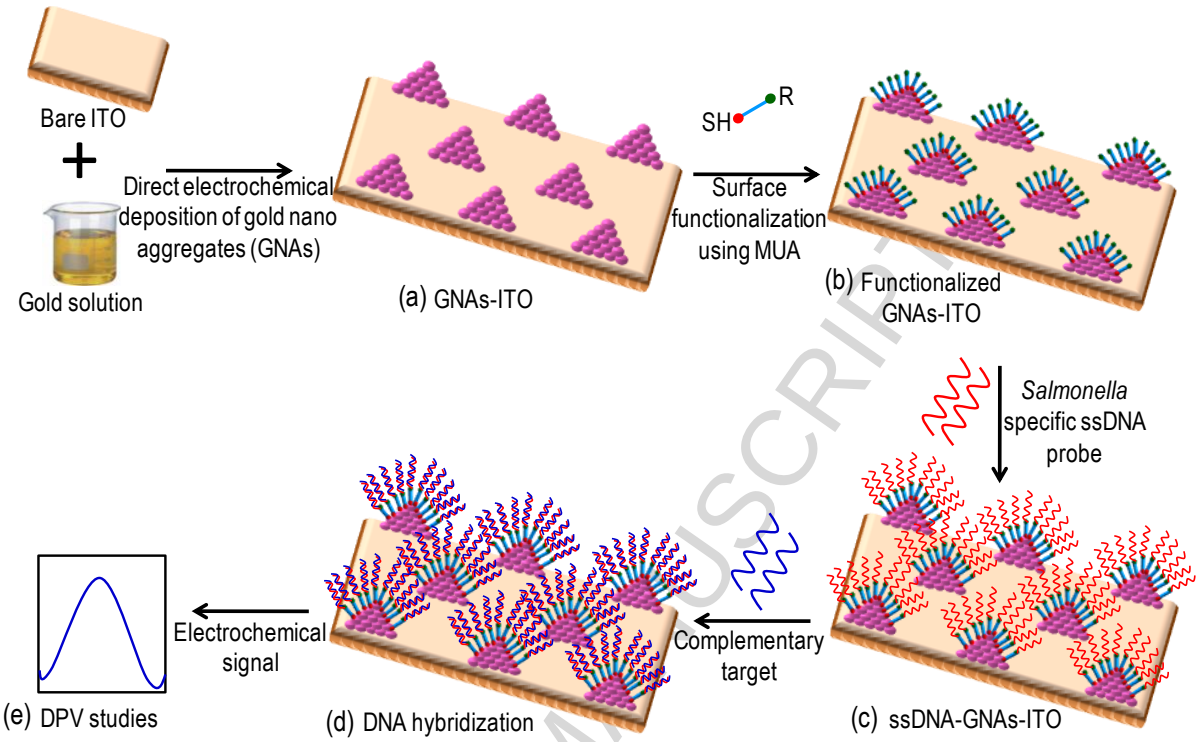

Scheme 1

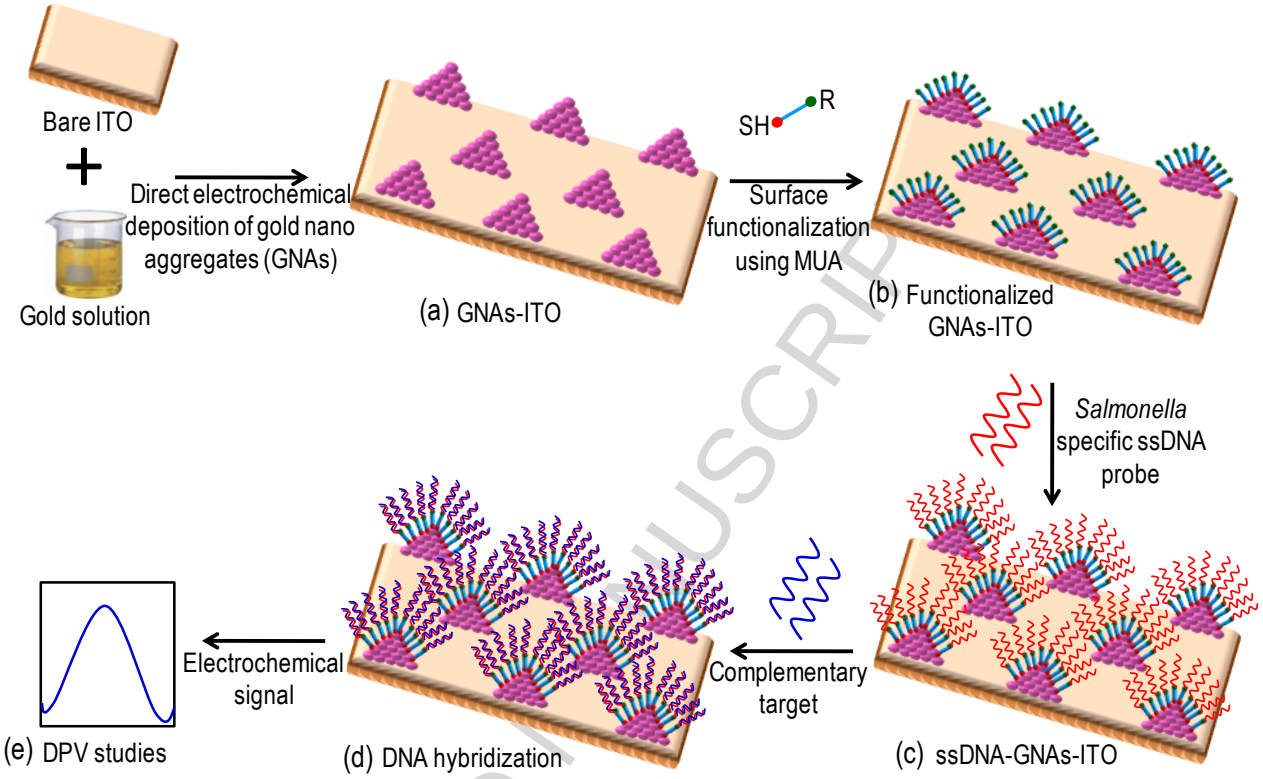

Fig.1

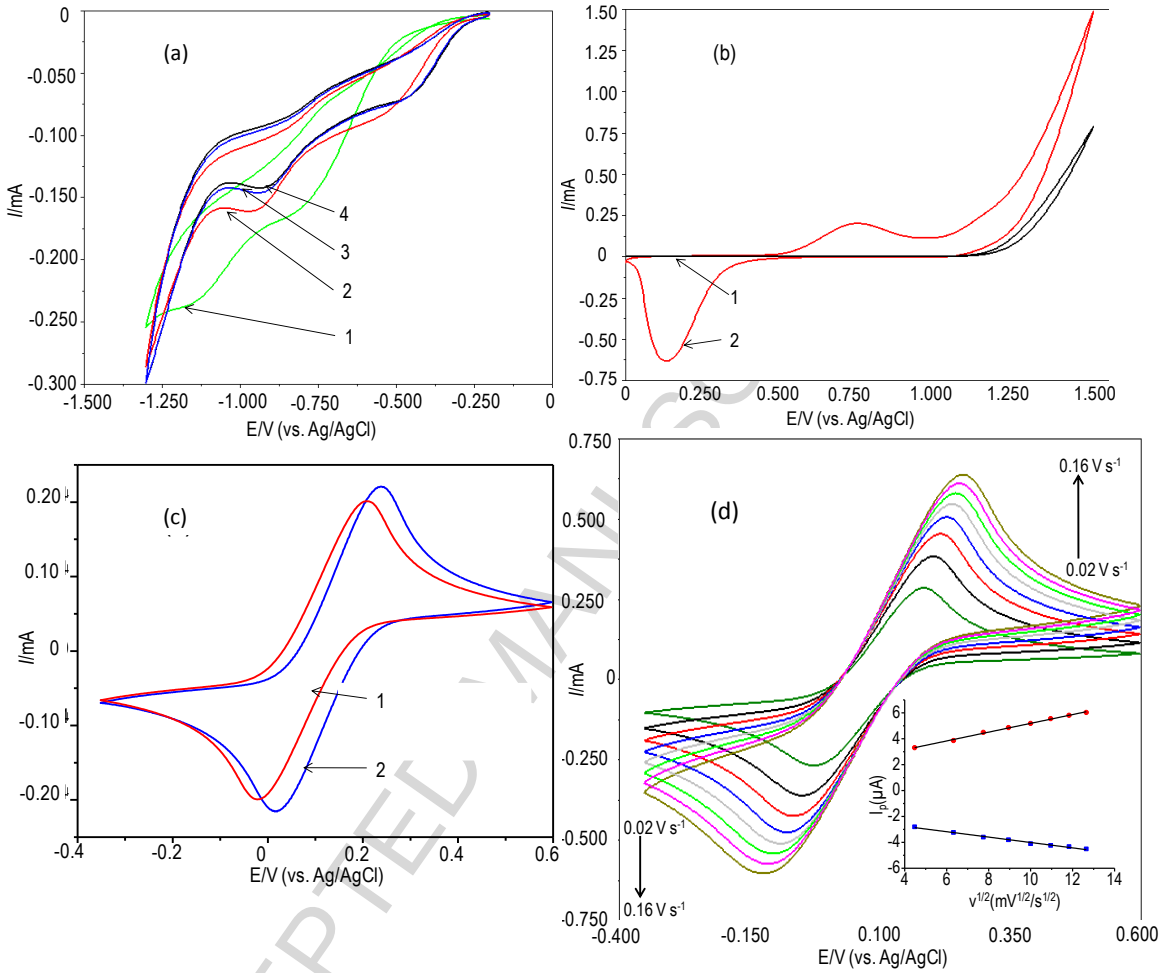

Fig. 2

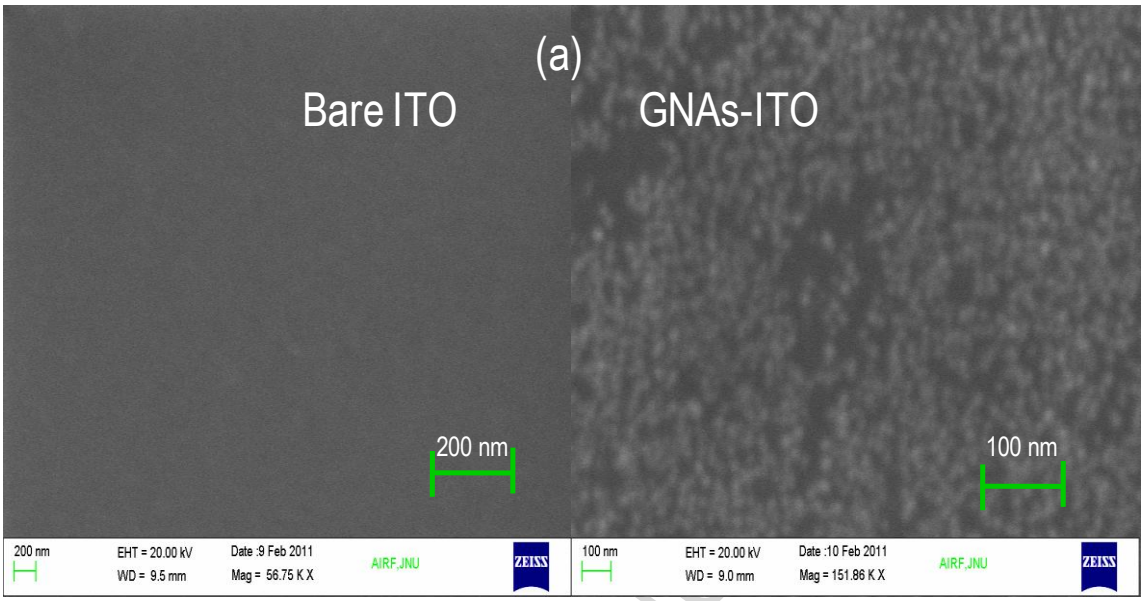

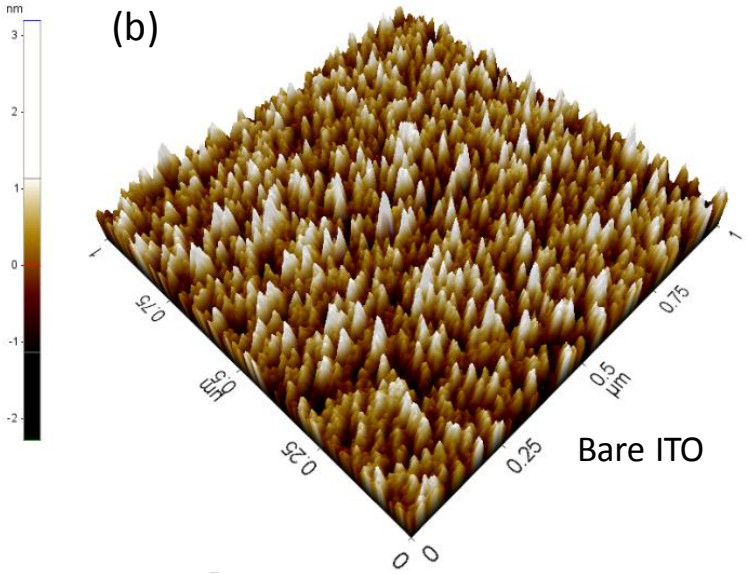

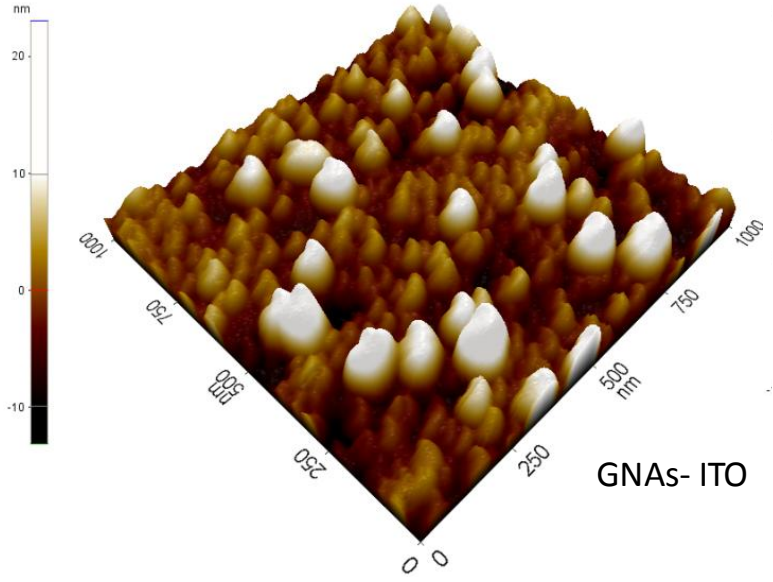

AFM data	Bare ITO	GNAs-ITO
Average roughness (nm)	0.081	1.589
Height of Islands (nm)	-	5-6
Average mean area of grains (nm)	-	7.367×10^{-3}
Average mean diameter of grains (nm)		1.44×10^{-2}

Fig. 3

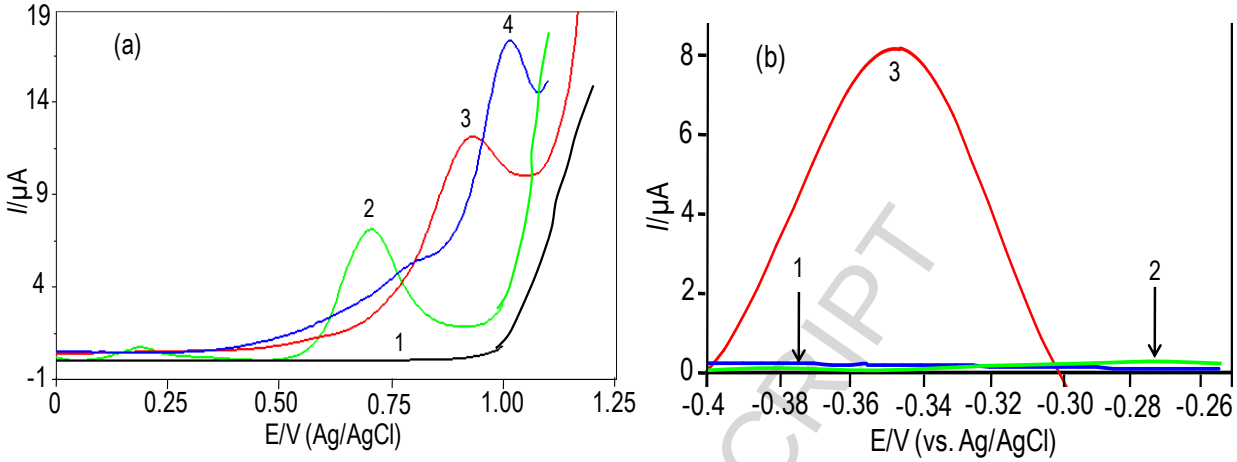

Fig. 4

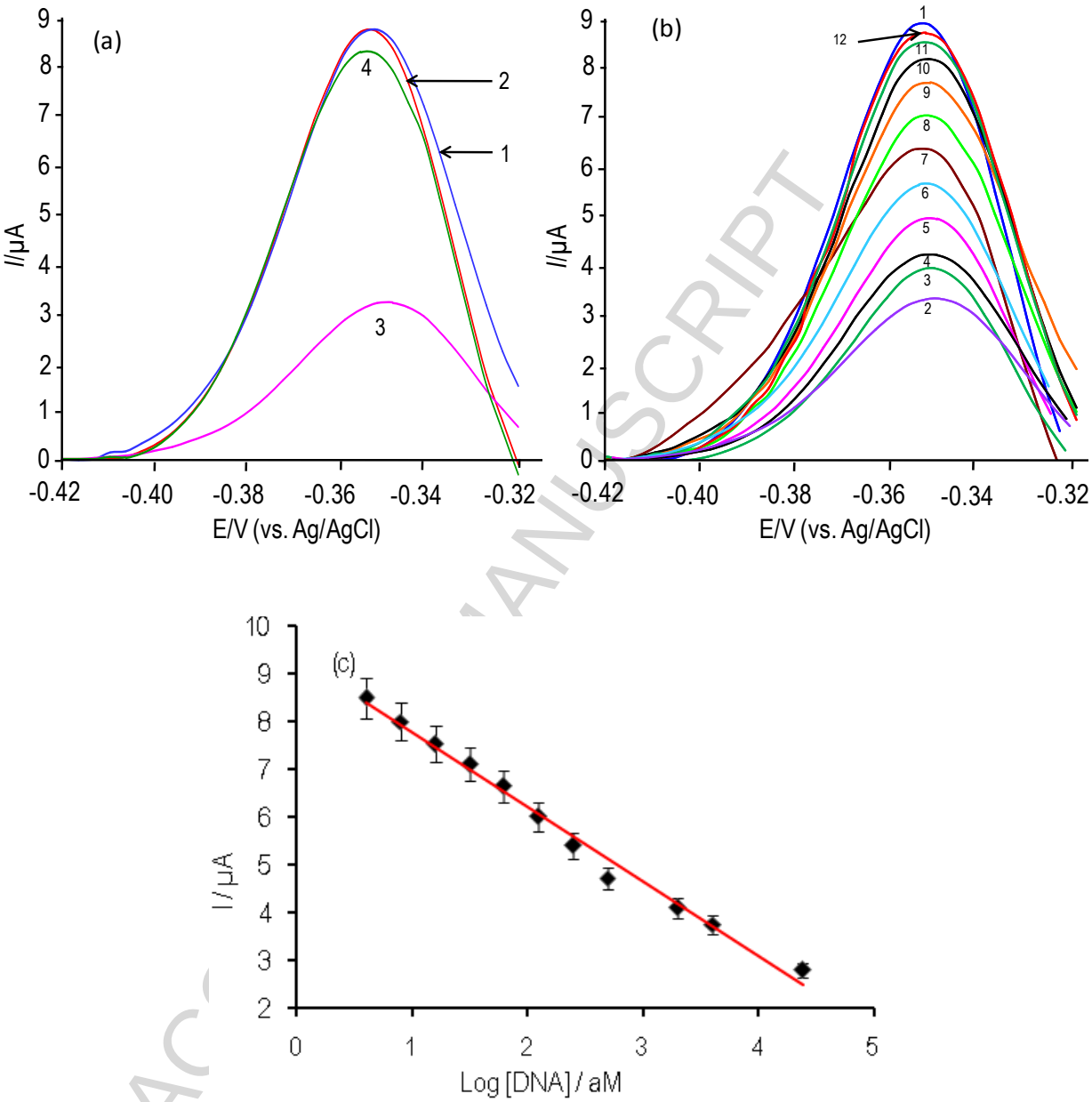

Fig. 5

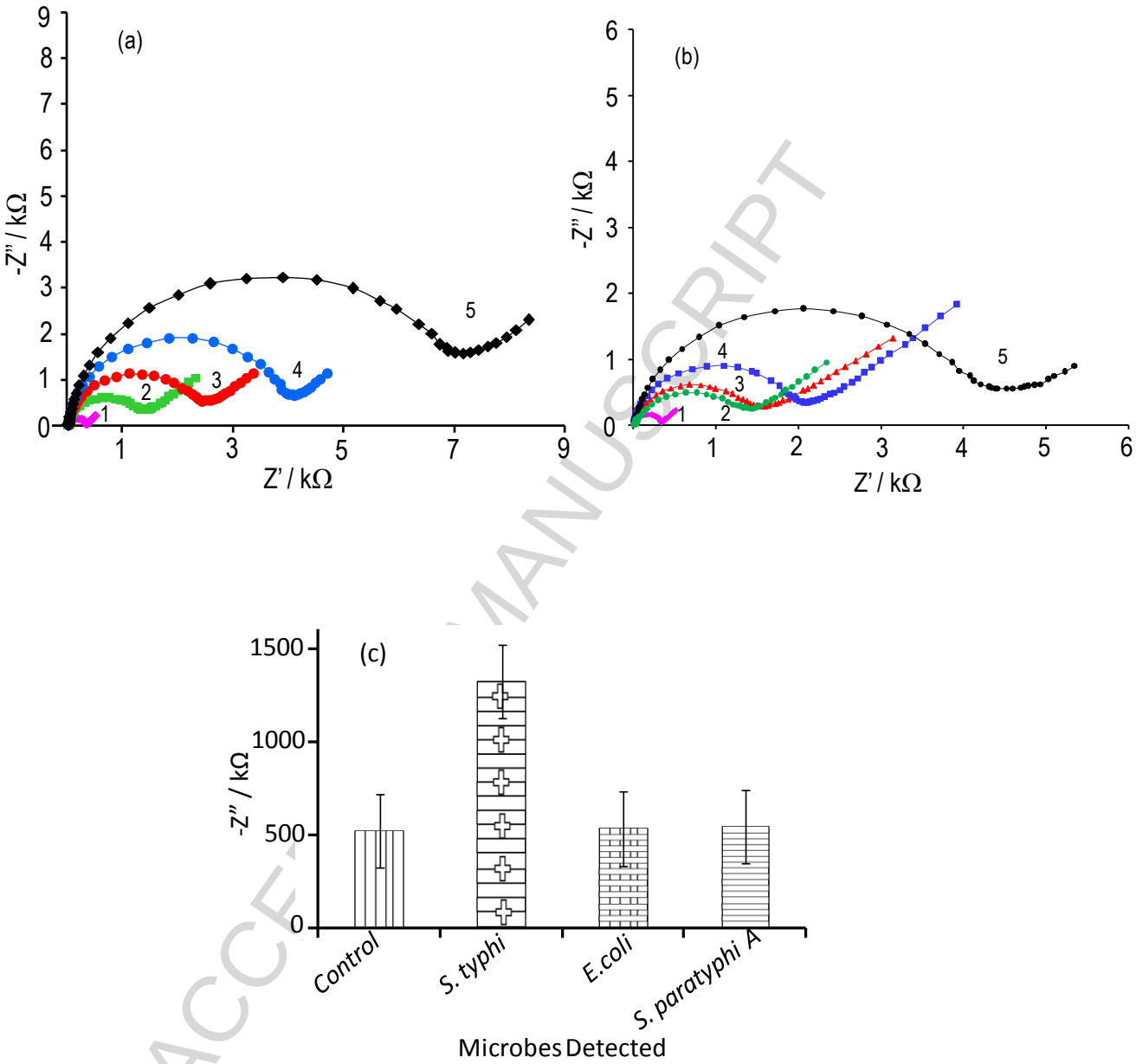

Table 1: Performances characteristics of various electrochemical DNA biosensors

S. No	Immobilization Matrix	Analyte	Dynamic Concentration Range	Detection Limit	Detection Technique	Detection Time/min	Ref
1	CTS-V_2O_5 - MWCNTs/CILE (a,b,c,)	*Y. enterocolitica* gene sequence	0.1 pM – 1.0 µM	1.7 pM	DPV with MB	10	27
2	PANI-NF-AuNP (d,e,f)	complementary strand of *S. aureus*	150 pM – 1 µM	150 pM	CV with MB	-	28
3	PANIw/graphene/GCE (g)	complementary DNA sequences	2.12 µM - 2.12 pM	32.5 pM	DPV with Daunomycin	-	29
4	[EMIM][Otf]/ZnO/CHIT/AuE (h,I,j)	complementary strand of *T. harzianum*	1 aM – 0.182 mM	0.1 aM	CV with MB	60	30
5	NAS-Modified Acrylic Microspheres (k)	Complementary DNA	0.1 fM - 100 µM	94.6 aM	DPV using anthraquninone -2-sulfonic acid monohydrate sodium salt	30	31
6	GO-CHI/ITO (l)	complementary strand of *S. typhi*	10 fM - 50 nM	10 fM	DPV with MB	1	32
7	AuNPs/CA/nBDD (m)	complementary DNA sequences	0.158 pM - 0.158 µM	9.8 pM	DPV with Daunomycin	-	33
8	PEDOT-PSS/AgNPs/AuE (n,o)	complementary sequence of *Ganoderma boninense*	1.0 fM - 1.0 nM	0.5 fM	DPV with ruthenium complex	25	34
9	Au NRs-GO nanocomposite (p)	complementary DNA sequences	1.0 nM – 10 fM	3.5 fM	DPV with MB	40	35
10	rGO–AuNPs	DNA insertion sequence IS6110 of *M. tuberculosis*	1 fM - 1 nM	1 fM	DPV using Au–PANI tracer	120	36
11	ZnONWs/Au Electrode(q)	breast cancer 1 gene	10.0 - 100.0 µM	3.32 µM	DPV	90	37
12	AuNPs/MoS_2/Gr/GCE (r)	complementary DNA sequences	50 fM - 5.0 nM	2.2 fM	DPV using SA-HRP-AuNPs tracer	90	38
13	MUA functionalized GNAs/ITO	complementary strand of *S. typhi*	4 aM - 24 fM	4 aM	DPV with MB	1	Present study

Highlights

- Realization of highly sensitive genosensor on direct electro-deposited gold nanoaggregates (non-toxic at physiological pH).
- Dynamic detection range of 4 aM- 24 fM of target DNA within 60s hybridization time using ssDNA-GNAs-ITO bio-electrode.
- Stability of bio-electrode more than 60 days and reusability upto 6 times.
- Successful detection of *S. typhi* in spiked urine and blood samples without using PCR amplification.